Jointly published by
Akadémiai Kiadó, Budapest
and Springer, Dordrecht

React.Kinet.Catal.Lett.
Vol. 96, No. 2, 379–389 (2009)
10.1007/s11144-009-5527-3

RKCL5527

SYNTHESIS AND CHARACTERIZATION OF NICKEL CATALYSTS SUPPORTED ON DIFFERENT CARBON MATERIALS

András Sápi[a], Róbert Rémiás[a], Zoltán Kónya[a]*, Ákos Kukovecz[a], Krisztián Kordás[b] and Imre Kiricsi[a]

[a]University of Szeged, Applied and Environmental Chemistry Department
6723 Szeged, Rerrich Béla tér 1.
[b]Microelectronics and Materials Physics Laboratories, Department of Electrical and Information Engineering, University of Oulu, P.O. Box 4500, 90014 Oulu, Finland

Received January 26, 2009, in revised form February 5, 2009, accepted February 6, 2009

Abstract

Nickel catalysts supported on various carbon materials such as multiwall carbon nanotubes, shortened length carbon nanotubes, graphite and amorphous carbon were synthesized, characterized and tested in cyclohexene hydrogenation reaction. We have found that carbon nanotube supports are superior to graphite and amorphous carbon both in terms of catalytic activity and stability.

Keywords: Nickel nanoparticles, carbon nanotubes, catalytic hydrogenation

INTRODUCTION

Carbon nanotubes (CNTs) have high thermal stability and are resistant against various corrosive chemicals. The porous microstructure of aligned bulk and disordered powder samples allows easy transport of reactants and products through the inter-tubular space thus carbon nanotubes hold promise for catalyst support applications [1,2]. When comparing the catalytic activity of metal catalysts on various carbonaceous materials, carbon nanotubes have often proved to be the best support. This is the case for the multiwall carbon nanotube (MWNT) supported platinum catalyst in (i) the catalytic wet air oxidation of nitrogen containing compound [3], (ii) the oxidation of environmentally harmful organic compounds to CO_2 [4], (iii) hydrogen generation from ammonia

* Corresponding author. E-mail: konya@chem.u-szeged.hu

0133-1736/2009/US$ 20.00.

[5] and (iv) isopropyl alcohol dehydrogenation [6]. Similar results were found for potassium doped ruthenium supported on MWNTs in ammonia synthesis [7]. Guczi and coworkers investigated selectivity changes in the Fischer-Tropsch (FT) reaction over MWNT-supported cobalt and iron catalysts [8]. A series of other Fe/CNTs catalysts have also been tested in Fischer-Tropsch synthesis [9]. For a review on the use and possible role of carbon nanotubes in heterogeneous catalysis we refer to reference [10]. The majority of the available studies rely on multiwall carbon nanotubes as supports for the deposited catalytic components. Nhut and coworkers reported an interesting example of the utilization of carbon nanotubes as nanoreactors [11] applied for the production of 1D zeolite crystals and the decomposition of H_2S in their interior.

Nanotube-supported metal catalysts can also be utilized for the production of carbon nanotubes or nanofibers. Cuoung Pham-Huu *et al.* described a large-scale synthesis method for the production of carbon nanofibers by catalytic chemical vapour deposition (CCVD) of ethane over carbon nanotubes supported nickel catalyst [12]. Singlewall carbon nanotubes have been investigated as support material for transition metal catalysts in the production of carbon nanotubes by CCVD [13,14]. Nickel and cobalt metals were anchored on MWNTs to investigate the influence of the particle size [15,16]. These literature data prove the increasing interest for carbon nanotubes as support for metal catalysts.

The aim of this work was to investigate the physico-chemical properties of nickel catalysts supported on different types of carbon materials such as multiwall carbon nanotubes, shortened length carbon nanotubes, graphite and amorphous carbon. We expect to gain a better understanding of the characteristics of these carbonaceous materials and their influence on the activities of supported metal catalysts.

EXPERIMENTAL

Carbon supports

Multiwall carbon nanotubes were produced by catalytic chemical vapour deposition (CCVD) of acetylene over a supported iron-cobalt bimetallic catalyst. The catalyst (freshly precipitated alumina containing 2.5% cobalt acetate and 2.5% iron(II) acetate) was placed onto a quartz boat positioned in the hot zone of a quartz reactor tube and nitrogen was introduced into the reactor while the temperature was increased to 700°C. At this temperature pure nitrogen was changed to a mixture of acetylene (30 cm^3/min) and nitrogen (270 cm^3/min). The chemical decomposition of acetylene took place under these conditions. After 30 min the generation of multiwall carbon nanotubes was completed, the acetylene stream was shut off and the reactor was cooled in nitrogen flow. The raw product was suspended in NaOH solution in order to

remove the alumina support then washed with distilled water. The metal catalyst particles formed at the beginning of the synthesis procedure were dissolved in diluted acid solution. The amorphous carbon species generally accompanying the formation of the carbon nanotubes were removed by oxidation using potassium permanganate in acidic media as described elsewhere [17]. The sample was finally washed with distilled water to neutral pH and dried in air.
The short-length MWNT sample was produced by ball-milling (using 10 steel balls in a 1000 ml steel vessel) at room temperature in air atmosphere for 12 hours [18]. The average length of MWNTs decreased to around 300 nm.

Graphite (a commercial product purchased from Sigma-Aldrich) and activated amorphous carbon (Fluka product) were used without further purification.

Preparation of nickel-loaded samples

A simple impregnation method was applied to deposit the nickel precursor (nickel acetylacetonate) onto the carbonaceous materials (multiwall carbon nanotube (MWNT), ball-milled multiwall carbon nanotubes (BM-MWNT), graphite (GR) and amorphous activated carbon (AC)) dehydrated at 105°C for 4 h. The predetermined amount of metal salts (to get a 5.5 w.% of metal content in the final products) was dissolved in benzene and the calculated amount of carbon supports was added to the solutions. After sonication and stirring the suspensions were heated in an inert atmosphere while stirring until the solvent evaporated completely. The product was dried at 105°C for 1 h then calcined in air at 185°C below the melting point of nickel acetylacetonate for 2 h. Finally the samples were heat treated at 380°C for 1 h to decompose the acetylacetonate and to get rid off any remaining adsorbates. The samples are labeled as NiO/MWNT, NiO/BM-MWNT, NiO/GR and NiO/AC.

The samples were reduced in hydrogen at 350°C for 1 h in order to convert nickel oxide to metallic nickel. The resulting catalyst samples are denoted Ni/MWNT, Ni/BM-MWNT, Ni/GR and Ni/AC. The nominal compositions of the samples are summarized in Table 1.

Sample characterization

The samples were characterized by different physico-chemical methods. The morphology of the samples was characterized by transmission electron microscopy (TEM – EFTEM LEO 912 OMEGA and Philips CM10). For investigation of surface characteristics BET measurements were carried out (QuantaChrome 2200). The crystal structure of supported nickel samples was studied by XRD (Rigaku Miniflex II). Electron diffraction patterns have also been investigated and evaluated using the Process Diffraction computer

program [19]. The activity of the samples was tested in the catalytic hydrogenation of cyclohexene (CH) in a continuous flow system by a time-on-stream test carried out at 50°C with a CH/H_2 mixture (at $CH:H_2$ = 1:4 and 1:9 ratios to determine the effect of variation in the ratio of the reacting gases) Activity studies were also performed by temperature programmed reaction (TPR) in the temperature range of 50-280°C using a CH/H_2 = 1:4 mixture with a flow rate of 10 cm^3/min and a 2°C/min temperature ramp. Before each catalytic reaction the catalysts were pre-activated in H_2 gas with a flow rate of 30 cm^3/min at 350°C for 1 h.

RESULTS AND DISCUSSION

N_2 adsorption measurements

The unloaded support materials used in our experiments showed different structures and crystallinity. Carbon nanotubes featured tubular graphite layer structures while active carbon was amorphous. Beside these morphological differences the specific surface areas of samples were also different. Values in Table 1 show the BET surface areas of the metal-loaded samples. The carbon nanotube supported sample had a surface area of 275 m^2/g and, therefore, it occupies an intermediate position between amorphous carbon and graphite supports. The Ni/BM-MWNT sample has somewhat smaller value (237 m^2/g). As the nominal nickel loadings are identical (5.5 wt.%) the density of metal particles on different surface areas should be different.

Table 1

BET Surface areas of the different catalysts

Catalyst	Ni content (wt.%)	Surface area (m^2g^{-1})
Ni/MWNT	5.5	275
Ni/BM-MWNT	5.5	237
Ni/GR	5.5	3
Ni/AC	5.5	650

TEM study

Characteristic TEM images of the samples are presented in Fig. 1. The MWNT sample featured nanotubes of different lengths but rather uniform diameter. In the image of the loaded but unreduced sample (Fig. 1/b) the NiO particle size distribution appears centered at 5.6 ± 1.6 nm. No visible changes

are observable in the density of the nickel particles in the image taken after reduction in hydrogen atmosphere. However the particle size distribution has narrowed (maximum at 5.6 ± 0.6 nm) as shown in the inset of Fig. 1/c.

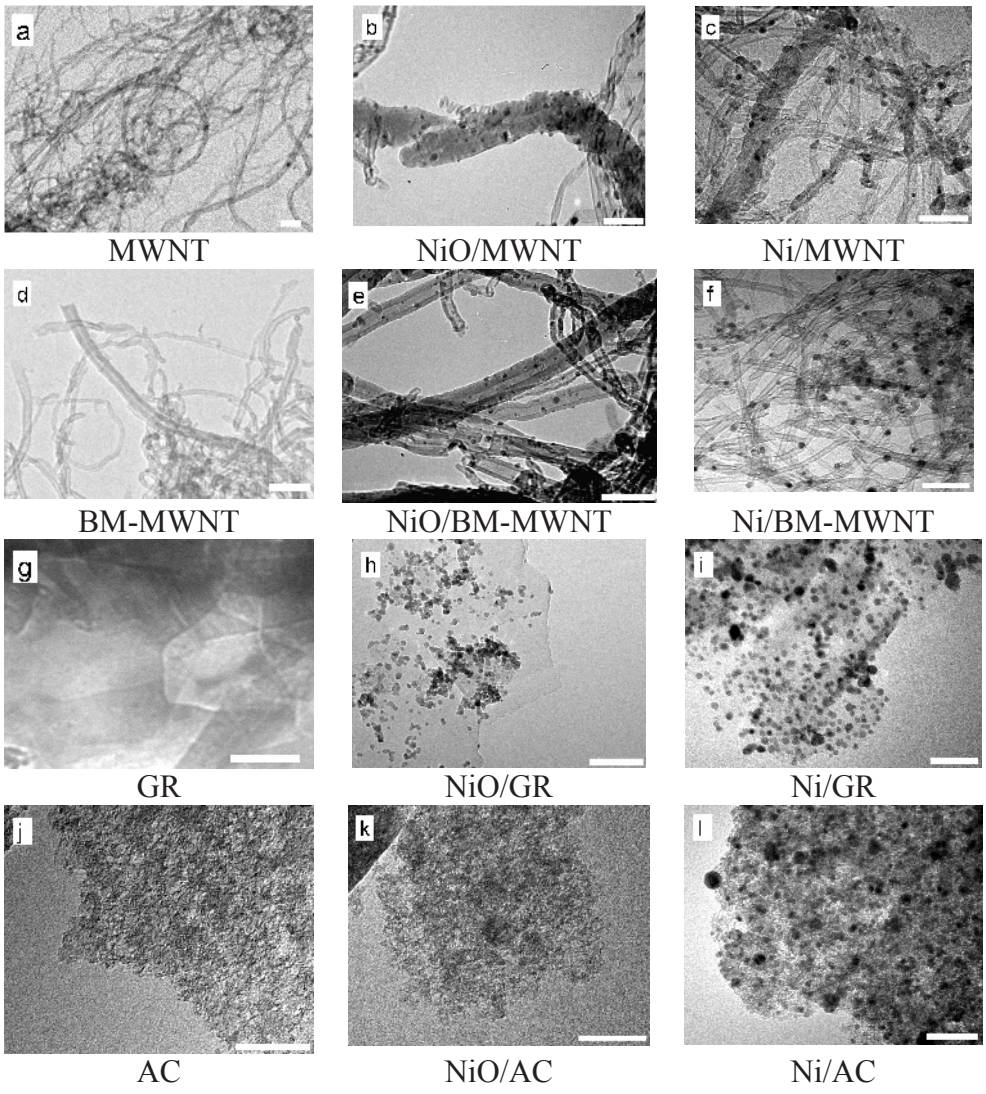

Fig. 1. TEM images of the different samples (scale bar is 50 nm in every case)

The TEM image of the ball-milled nanotube sample reveals two clearly visible features: the nanotube ends are open and their length is somewhat shorter due to the breaking the original nanotubes. A third characteristic feature is also observable for the ball-milled MWNTs: milling-induced surface imperfections on the outer shells could be identified in agreement with previously published results [20]. The dangling bonds at the open tube ends and at the surface vacancies are saturated by –COOH, -OH and =CO groups [21]. The loaded sample (Fig. 1/e) shows NiO nanoparticles with an average diameter of 3.1 ± 1.2 nm. Visual inspection of the TEM image of the corresponding reduced sample (Fig. 1/f) reveals that the particles became larger and more uniform in diameter during the treatment. This is also evidenced by the particle size distribution calculated from the TEM images (average particle size 6.2 ± 1.0 nm). The increase can be traced back to the agglomeration of the smaller particles and their anchoring onto the surface – most probably at the defect sites. The lamellar structure of graphite is seen in Fig. 1/g. After decomposition of the impregnated nickel acetylacetonate salt, small and uniform nanoparticles form on the support (3.5 ± 1.1 nm), which become somewhat larger after reduction in hydrogen (5.6 ± 1.6 nm), most probably due to the high mobility of Ni on the smooth graphite surface.

The amorphous active carbon sample showed an interesting behavior in terms of crystal formation on its surface. When decomposing the Ni precursor at 380^{o}C, no any anchored particles could be detected by TEM (Fig. 1/k). However, after reduction in hydrogen atmosphere, nickel particles with an average size of 6.7 ± 2.4 nm appeared in the sample. A possible explanation for this is that due to the large surface area of this support the nickel acetylacetonate precursor was very evenly distributed, and there was no surface force to aggregate the NiO moieties into larger, TEM-detectable species. However, after reduction in hydrogen atmosphere nickel particles of considerable sizes have appeared. The average particle size was found to be 6.7 ± 2.4 nm. Both the size (6.7 nm) and the deviation (2.4 nm) for this sample are the largest values found among the tested supported nickel materials.

XRD measurements

XRD patterns of the unloaded original support materials, the decomposed samples, as well as the reduced samples are shown in Fig. 2. For MWNT and its ball-milled derivative an intensive reflection is seen at d = 0.340 nm, being characteristic of the C(002) sheet of graphitic layers. This XRD feature of MWNTs is well known in the literature and assigned to the rolled graphene sheets [22]. The more crystalline graphite also gives this reflection at d = 0.334 nm. However, the characteristics of the graphite profile indicate a crystalline structure insofar as this reflection is more intense here and its half-width is much smaller than those of MWNT samples. Besides this very

intensive reflection, two additional signals corresponding to C(100) and C(004) also appeared at d = 0.207 nm and 0.171 nm values, respectively. The C(002) reflection is broad and centered at d = 0.340 nm revealing that structural units with long-range ordering do not exist in this sample.

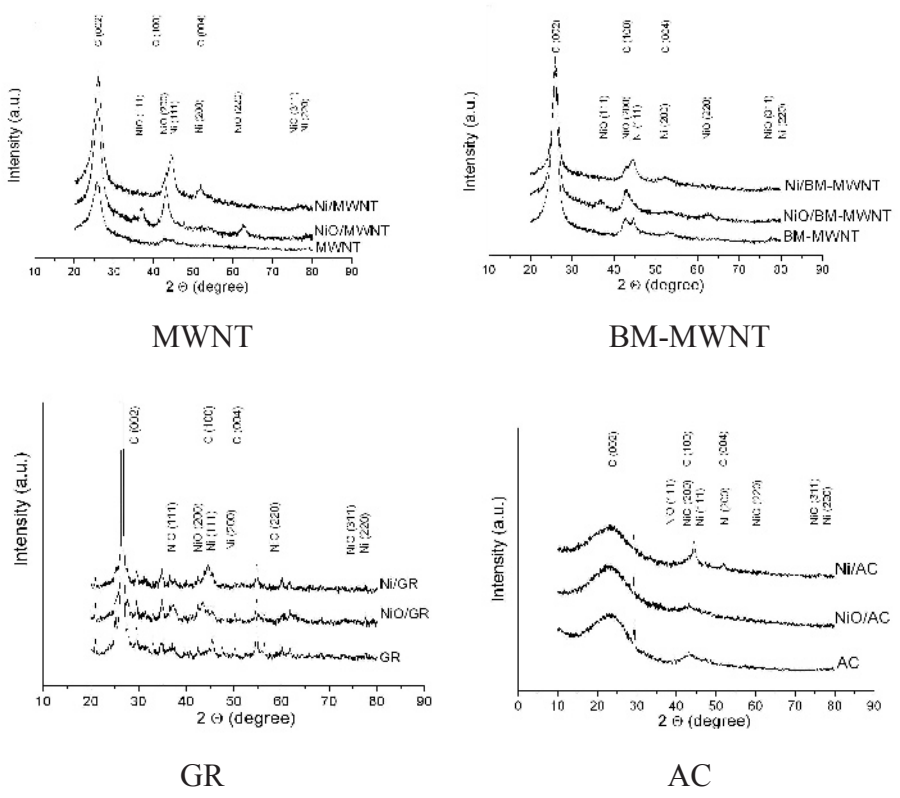

Fig. 2. XRD profiles of the different catalysts

XRD patterns measured after loading the carbon materials with nickel acetylacetonate and decomposing the salt, characteristic reflections for NiO were found. A notable exception is the amorphous carbon support where no NiO could be identified. We assume that in this case the nickel acetylacetonate was so finely dispersed on the high surface area support that no particles detectable by XRD could be formed upon the thermal treatment of the precursor salt – being in a good agreement with the results of the independent TEM investigation.

Reflections characteristic of Ni were found in each XRD pattern of the reduced samples. The Ni(111) reflection appeared as an intensive signal at

d = 0.209 nm. The size of nickel nanoclusters was determined using the Scherer equation and is presented in Table 2. It is interesting to note that the TEM-derived and XRD-derived particle sizes are similar but not identical for the samples.

Table 2

Particles size of the NiO and Ni nanoparticles

	Average diameter (nm)			
	NiO		Ni	
Support	TEM	XRD	TEM	XRD
MWNT	5.6 ± 1.6	7.4 ± 0.4	5.4 ± 0.7	5.6 ± 0.3
BM-MWNT	3.1 ± 1.2	3.8 ± 0.4	6.2 ± 1.0	7.7 ± 0.3
AC	n.a.	n.a.	6.7 ± 2.4	8.6 ± 0.7
GR	3.5 ± 1.1	5.9 ± 0.3	5.6 ± 1.6	10.6 ± 0.2

Catalytic activity

The results of the time on stream tests on all four Ni/Carbon catalyst materials are presented in Fig. 3. The solid black vertical lines indicate the time when the ratio of the reaction mixture was switched from $CH:H_2$ = 1:9 to 1:4. The activated MWNT-supported catalysts showed excellent long-lived activity. Initial conversion on the Ni/MWNT catalyst was 100% and deactivation only started after 8 h time-on-stream, whereas Ni/BM-MWNT still featured 100% conversion even after 16 h on stream. In the case of Ni/AC catalyst the maximum conversion (50%) rapidly decreased after 1 h on stream. Initial conversion on the Ni/GR catalyst was low at 4% and gradually decreased further during the whole reaction.

It can be seen that conversions increased on both Ni/MWNT and Ni/AC catalysts when the dilution of the reaction mixture with H_2 was stopped. This can be explained by the increased residence time of cyclohexene in the reactor.

Figure 4 shows the results of the TPR study for investigating the competition of the hydrogenation to cyclohexane and dehydrogenation to benzene reactions in case of all four catalysts. It can be seen that dehydrogenation outrivals hydrogenation at 504 K over the MWNT supported catalyst while the same phenomenon comes forth at 496 K and 579 K over Ni/AC and Ni/GR, respectively. In case of the Ni/GR, the changes in the slope of selectivity can be explained by assuming the onset of a new reaction with different mechanism at 530 K.

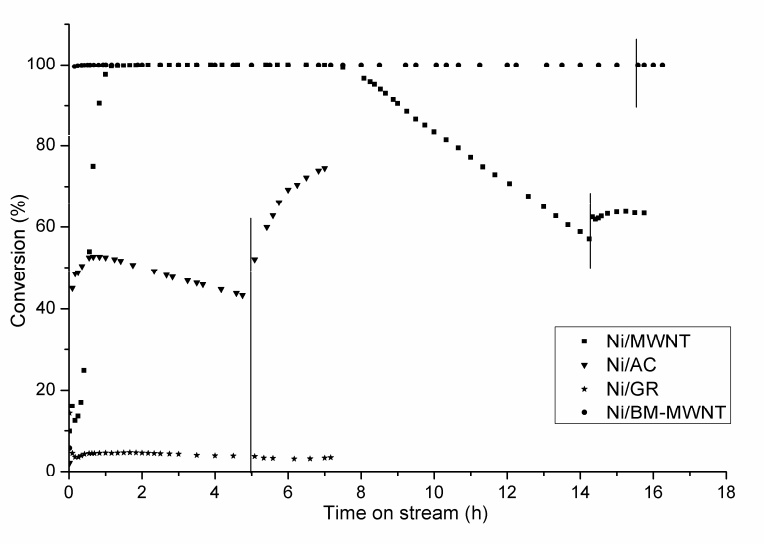

Fig. 3. Time-on-stream stability of various catalysts in the hydrogenation of cyclohexene to cyclohexane

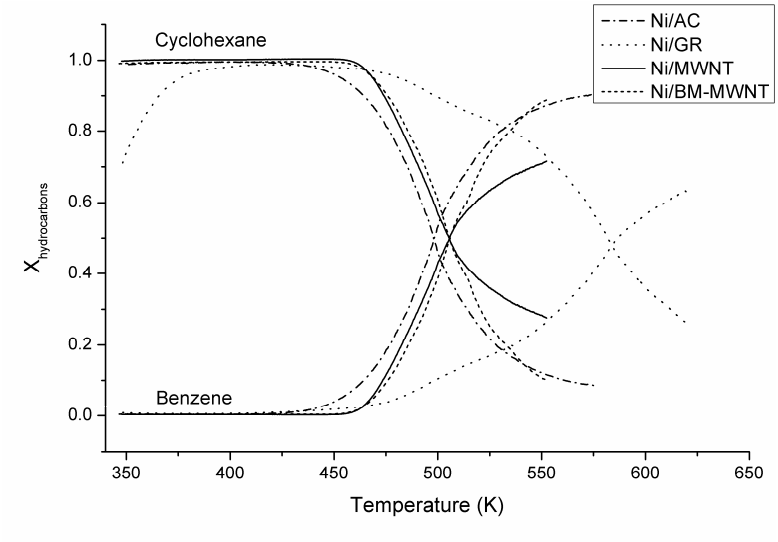

Fig. 4. Temperature programmed reaction curves (upper curves: cyclohexane formation, lower curves: benzene formation)

CONCLUSIONS

It has been demonstrated that carbon supported Ni catalysts are active in the hydrogenation/dehydrogenation reactions of cyclohexene. It was shown that the sizes of the obtained NiO and Ni nanoparticles are strongly dependent on the support. Since the hydrogen spillover effect is the driving force in the surface reactivity of nickel catalysts supported on different forms of carbon and the electronic properties of the applied carbonaceous supports are very different from each other, it is obvious that the catalytic behavior of the prepared catalysts is also quite dissimilar.

In order to control the hydrogen spillover effect on the prepared catalysts, we have to find the optimum combination of metal atom reactivity, strength of metal-support interaction, and range of specific surface area.

Acknowledgement. This work was supported by the Hungarian Research Fund OTKA K73676 and the FP6 STREP "SANES" (017310). K.K. is acknowledging funding received from the Academy of Finland (120853, 124357, 128626) and from Tekes (52423, 52433).

REFERENCES

1. W. Li, C. Liang, W. Zhou, J. Qui, Z. Zhou, G. Sun, Q. Xin: *J. Phys. Chem. B*, **107**, 6292 (2003).
2. M. Carmo, V.A. Paganin, J.M. Rosolen, E.R. Gonzalez: *J. Power Sources*, **142**, 169 (2005).
3. J. Garcia, H.T. Gomes, P. Serp, P. Kalck, J.L. Figueiredo, J.L. Faria: *Catal. Today*, **102-103**, 101 (2005).
4. H.T. Gomes, P.V. Samant, Ph. Serp, Ph. Kalck, J.L. Figueiredo, J.L. Faria: *Appl. Catal. B: Env.*, **54**, 175 (2004).
5. S.-F. Yin, Q.-H. Zhang, B.-Q. Xu, W.-X. Zhu, C.-F. Ng, C.-T. Au: *J. Catal.*, **224**, 384 (2004).
6. K. Niesz, A. Siska, I. Vesselenyi, K. Hernadi, D. Mehn, G. Galbacs, Z. Konya, I. Kiricsi: *Catal. Today*, **76**, 3 (2002).
7. H.-B. Chen, J.-D. Lin, Y. Cai, X.-Y. Wang, J. Yi, J. Wang, G. Wei, Y.-Z. Lin, D.-W. Liao: *Appl. Surf. Sci*., **180**, 328 (2001).
8. L. Guczi, G. Stefler, O. Geszti, Zs. Koppány, Z. Kónya, É. Molnár, M. Urbán, I. Kiricsi: *J. Catal*., **244**, 24 (2006).
9. M. C. Bahome, L. L. Jewell, D. Hildebrandt, D. Glasser, N. J. Coville: *Appl. Catal. A: Gen.*, **287**, 60 (2005).
10. Ph. Serp, M. Corrias, Ph. Kalck: *Appl. Catal. A: Gen.*, **253**, 337 (2003).
11. J.-M. Nhut, L. Pesant, J.-P. Tessonnier, G. Wine, J. Guille, C. Pham-Huu, M.-J. Ledoux: *Appl. Catal. A: Gen*., **254**, 345 (2003).
12. C. Pham-Huu, N. Keller, V.V. Roddatis, G. Mestl, R. Schlögl, M.J. Ledoux: *Phys. Chem. Chem. Phys*., **4**, 514 (2002).
13. K. Hernadi, L. Then-Nga, E. Ljubovic, L. Forro: *Chem. Phys. Lett*., **367**, 475 (2003).
14. C.-H. Li, K.-F. Yao, J. Liang: *Carbon*, **41**, 858 (2003).

15. H. Liu, G. Cheng, R. Zheng, Y. Zhao: *J. Mol. Catal. A: Chem.*, **225**, 233 (2005).
16. I. Kiricsi, Z. Konya, K. Niesz, A.A. Koos, L.P. Biro: *Proc. SPIE*, **5118**, 280 (2003).
17. Z. Konya: *NATO Sci. Ser. E*, **372**, 85 (2001).
18. N. Pierard, A. Fonseca, Z. Kónya, I. Willems, G. Van Tendeloo, J. B.Nagy: *Chem. Phys. Lett.*, **335**, 1 (2001).
19. J.L. Lábár: Proc. EUREM 12. Brno, **III**, 379 (2000).
20. Z. Kónya, J. Zhu, K. Niesz, D. Mehn, I. Kiricsi: *Carbon*, **42**, 2001 (2004).
21. Z. Kónya, I. Vesselenyi, K. Niesz, A. Demortier, A. Fonseca, J. Delhalle, Z. Mekhalif, J. B.Nagy, A.A. Koós, Z. Osváth, A. Kocsonya, L.P. Biró, I. Kiricsi: *Chem. Phys. Lett*., **360**, 429 (2002).
22. Y. Maniwa, R. Fujiwara, H. Kira, H. Tou, E. Nishibori, M. Takata, M. Sakata, A. Fujiwara, X. Zhao, S. Iijima, Y. Ando: *Phys. Rev. B*, **64**, 073105 (2001).